Structural Response Analysis and Fatigue Damage Estimation of a Floating Bridge Subjected to Inhomogeneous Wave Loads

Jian Dai[1], Bernt Johan Leira[1], Torgeir Moan[1], Hagbart Skage Alsos[2]
[1]Department of Marine Technology, Norwegian University of Science and Technology
Trondheim, Norway
[2]SINTEF Ocean
Trondheim, Norway

ABSTRACT

In this paper, a computational study of the structural responses of a floating bridge for crossing of the Bjørnafjord in Norway is presented. The study employs an idealized floating bridge model developed based on the phase 3 design concept which comprises a very long, straight and side-anchored floating bridge. Due to the very long span and complex topology, the local wind waves exhibit some inhomogeneities. This study investigates the effects of inhomogeneous wave loads on the global responses of the floating bridge. The structural responses of both the bridge girders and the mooring lines are presented and discussed. In addition, the short-term fatigue damage induced by inhomogeneous wave loads in the mooring lines is also evaluated.

KEY WORDS: Floating bridge; inhomogeneous waves; structural response; short-crested waves; fatigue damage.

INTRODUCTION

The Norwegian Public Road Authority (NPRA) initiated the E39 coastal highway project with the aim to significantly reduce the time for travel by road along the Norwegian coastline. The reduction in travel time will be mainly achieved by replacing time-consuming ferry trips across the fjords with road connections by means of bridges and/or tunnels. Owing to the fact that many fjords along the E39 highway route are very wide and deep, this brings challenges for constructing road connections across the fjord. For example, the combination of a span of up to 5 km and waters as deep as 500 m makes it very difficult for conventional bridges to cross the Bjørnafjord. Constructing floating bridges for this fjord crossing was soon identified as an appealing option because of their advantages of using natural buoyancy for load-carrying purposes and being less sensitive to seabed conditions as compared with other kinds of bottom-founded structures. Since then, many research activities related to the feasibility of floating bridge concepts across the Bjørnafjord have been carried out (Cheng et al., 2018a; Cheng et al., 2018b; Viuff et al., 2019; Xiang et al., 2018).

Although floating bridges have distinct advantages over other types of structures for crossing of the Bjørnafjord, the design of such structures is still technically challenging. For example, available field measurement data show that the wave field along the bridge crossing exhibits some inhomogeneities (Cheng et al., 2019a). This brings complications when it comes to the detailed modeling and analysis of the floating bridge. Although a common practice in engineering design is to apply the worst wave condition to the entire bridge structure, the literature shows that such an assumption could lead to underestimated responses in certain cases (Fylling, 2012). It is therefore important to include the inhomogeneity of wave conditions when examining the bridge responses.

In this paper, we present a numerical study of the dynamic responses of a floating bridge subjected to inhomogeneous wave loads. An idealized floating bridge model is employed based on the phase 3 design concept for the crossing of the Bjørnafjord. The bridge model comprises a 4.6 km long straight bridge girder resting on 35 evenly spaced pontoons. To limit the bridge response to the wave loads in the horizontal plane, four clusters of deep water mooring lines spaced 1 km apart are engaged to increase the transverse stiffness of the bridge. This study examines the various effects of inhomogeneous wave loads on the dynamic responses of the floating bridge. These inhomogeneities include the spatial variation of the wave direction, significant wave height as well as the coherence and correlation of waves along the entire length of the floating bridge. For the purpose of comparison, the case describing a homogeneous wave condition is also considered. In addition, the fatigue damage induced by inhomogeneous wave loads in the mooring lines is also evaluated and discussed.

NUMERICAL MODEL

The phase 3 design concept of the floating bridge across the Bjørnafjord is illustrated in Fig. 1. The design concept comprises a straight, side-anchored floating bridge section followed by a cable-stayed bridge section located at the south end. For the sake of simplification, in this study, we employ an idealized bridge model comprising a 4.6 km long straight bridge girder vertically supported by 35 evenly spaced pontoons. The bridge girder is elevated 18 m above the water surface. The water depth is taken as 300 m and is assumed to be constant throughout the entire length of the bridge. Four standardized clusters of deep water mooring lines are attached to four pontoons in order to limit the transverse response of the bridge. Figure 2 shows a schematic view of the floating bridge model. Note that the global x-axis refers to the longitudinal direction of the bridge.

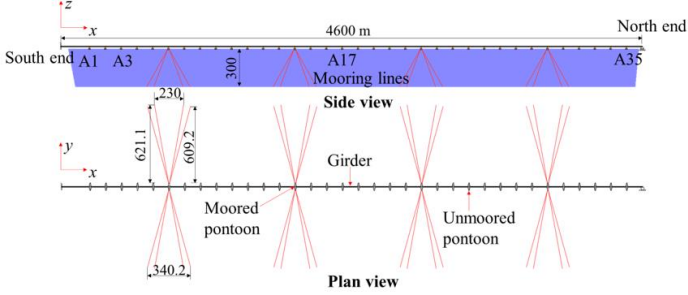Fig. 1: Floating bridge design concept across the Bjørnafjord (COWI, 2019)

Fig.2: Schematic view of idealized floating bridge model

In the numerical model, the steel bridge girder and the columns connecting the girder and pontoons are modeled as Euler beams. The mooring lines are composed of a wire segment sandwiched by top and bottom chain segments, and they are idealized as bars accounting for tensile forces only. All mooring lines are pretensioned. The pretensions for the internal mooring clusters and the end clusters are 1400 kN and 1522 kN, respectively. The pontoons are treated as large volume rigid bodies subjected to wave loads. At the bridge south end, all six degrees of freedom of the girder are fully restricted. At the north end, the longitudinal translation along the x-axis and the rotation about the z-axis are released to allow for deformations due to thermal effects. Table 1 lists some of the key structural properties of the floating bridge model. Note that a detailed description of the model has been documented in Dai et al. (2019). Also note that all the parameters adopted are based on available information obtained from independent studies of the bridge design concept (Multiconsult, 2017a; DNV GL, 2018).

Table 1. Properties of bridge structural components

Parameter	Value
Main girder weight	16040 kg/m
Main girder weak axis moment of inertia (I_y)	6.64 m^4
Main girder strong axis moment of inertia (I_z)	3.21 m^4
Column weight	9180 kg/m
Column sectional moment of inertia (I_x)	12.94 m^4
Column sectional moment of inertia (I_y)	14.92 m^4
Pontoon freeboard	3.5 m
Pontoon draft (unmoored)	5 m
Pontoon draft (moored)	8.5 m
Pontoon weight (unmoored)	850 ton
Pontoon weight (moored)	1452 ton
Mooring line diameter (top chain)	147 mm
Mooring line diameter (wire)	124 mm
Mooring line diameter (bottom chain)	147 mm

In the bridge model, pontoons are the key structural components interacting with water. For evaluation of the wave loads acting on the pontoons, the potential flow theory is employed. In view of the fact that the spacing between adjacent pontoons is large considering the relatively short waves in a fjord, the hydrodynamic interaction between pontoons is neglected. Then, the hydrodynamic coefficients (added mass and potential damping) and excitation force transfer functions corresponding to a single pontoon may be conveniently evaluated in the frequency domain. The equation of motion in the time domain can then next be established according to Cummins theory (Cummins, 1962) as

$$\sum_{j=1}^{6}\left(M_p + A_j^{\infty}\right)\ddot{u}_{pj}(t) + \int_{-\infty}^{\infty}\kappa_j(t-\tau)\dot{u}_{pj}(t)d\tau$$
$$+\left(K_j^h + K_j^b\right)u_{pj}(t) = F_j^{exc}(t) \tag{1}$$

where M_p is the pontoon mass, A_j^{∞} is the added mass corresponding to the jth degree of freedom at infinite frequency, κ_j is the retardation function, K_j^h represents the hydrostatic restoring stiffness, K_j^b is the stiffness from the bridge structure, u_{pj} is the relevant displacement component of the pontoon, and F_j^{exc} is the excitation force which contains the first order wave load F_j^{1st} and second order difference-frequency load component F_j^{2nd}. The viscous forces acting on pontoons are not considered in this study.

Besides pontoons, the mooring lines (when in motion) are also subjected to inertial and viscous forces due to the surrounding water. Such hydrodynamic loads may be conveniently computed according to Morison's equation as (Gudmestad and Moe, 1996)

$$f_b = \rho_w V\ddot{u}_w + \rho_w C_a V\left(\ddot{u}_w - \ddot{u}_m\right) + \frac{1}{2}\rho_w C_d D\left(\dot{u}_w - \dot{u}_m\right)\left|\dot{u}_w - \dot{u}_m\right| \tag{2}$$

where f_b is the transverse hydrodynamic load per unit length, ρ_w is the density of the water, V is the volume per unit length of the mooring line, D is the mooring line diameter, $\dot{u}_m$ is the transverse velocity of the mooring line, and correspondingly, $\dot{u}_w$ is the flow speed along the direction of $\dot{u}_m$, $C_a = 1$ is the added mass coefficient, and C_d, which equals 2.4 for chain segments and 1.2 for wire segments (Multiconsult, 2017b), is the quadratic drag coefficient.

Through finite element discretization and assemblage as well as considering the hydrodynamic components given in Eqs. (1) and (2), the global equations of motion of the entire floating bridge can be written in a compact matrix form as (Naess and Moan, 2012)

$$\mathbf{M\ddot{u}} + \mathbf{C\dot{u}} + \int_{-\infty}^{\infty}\mathbf{K}_R(t-\tau)\dot{u} + \mathbf{Ku} = \mathbf{F} \tag{3}$$

where $\mathbf{M}$ is the global mass matrix containing the added mass properties, $\mathbf{C}$ is the global damping matrix including both structural and hydrodynamic damping properties. Rayleigh damping with mass coefficient $\mu = 0.001$ and stiffness coefficient $\lambda = 0.025$ is adopted for the structural damping. $\mathbf{K}_R$ is the global matrix containing retardation functions for the degrees of freedom of pontoons only, $\mathbf{K}$ is the global stiffness matrix containing the hydrostatic restoring stiffness, $\mathbf{F}$ is the external load vector, and $\mathbf{u}$ is the displacement vector of the entire bridge structure. Note that the external load vector contains the gravitational forces, buoyancy forces and wave excitation forces.

In this study, we employ WAMIT (WAMIT, 2019) for computing the hydrodynamic coefficients and excitation force transfer functions in the frequency domain. These are next imported to SIMA for the global response analysis of the floating bridge model in the time domain through coupled RIFLEX-SIMO simulations (SINTEF Ocean, 2019a; SINTEF Ocean, 2019b). Note that the study focuses on the various

effects of inhomogeneous waves. Other environmental efforts, such as water current and wind, are not accounted for. This study also does not consider traffic loads.

INHOMOGENEOUS WAVE CONDITIONS

According to the available field measurement data (Cheng et al., 2019a), the wave conditions along the crossing of the Bjørnafjord are inhomogeneous. However, the data were collected from the three Datawell Wave Riders (DWRs) deployed close to pontoons A4, A13 and A27, respectively. With the relatively long distance between buoys and the limited number of buoys, a detailed description of the inhomogeneous wave field is not possible. Nevertheless, the inhomogeneous wave conditions may still be properly modeled by first assuming that the wave conditions in the vicinity of any individual pontoon are homogeneous, as illustrated in Fig. 3. Essentially, this means that the sea state around various pontoons could have different characteristics. According to the design basis (Statens vegvesen, 2018), the JONSWAP spectrum fits the locally wind generated wave conditions and thus the spectrum for short-term wind waves may be written as

$$S_\varsigma^j(\omega,\theta) = S_\varsigma^j(\omega) D_\varsigma^j(\theta) \tag{4}$$

$$S_\varsigma^j(\omega) = \frac{5}{16} A_\gamma H_s^2 \frac{\omega_p^4}{\omega^5} e^{-\frac{5}{4}\left(\frac{\omega}{\omega_p}\right)^{-4}} \gamma^{e^{-\frac{1}{2}\left(\frac{\omega-\omega_p}{\sigma\omega_p}\right)^2}} \tag{5}$$

$$D_\varsigma^j(\theta) = \frac{\Gamma\left(1+\frac{n}{2}\right)}{\sqrt{\pi}\Gamma\left(\frac{1}{2}+\frac{n}{2}\right)} \cos^n\left(\theta-\theta_p\right) \tag{6}$$

where $S_\varsigma^j(\omega)$ denotes the unidirectional wave spectrum at the jth pontoon, $A_\gamma = 1 - 0.287\ln(\gamma)$, ω_p is the peak angular frequency, γ is the non-dimensional peak shape parameter, σ is the spectrum width parameter which equals 0.07 for $\omega \le \omega_p$ and 0.09 for $\omega > \omega_p$, $D_\xi^j(\theta)$ is the directional spreading function, and n is the spreading coefficient which is set to 4 in this study as the wind waves are short-crested in the Bjørnafjord.
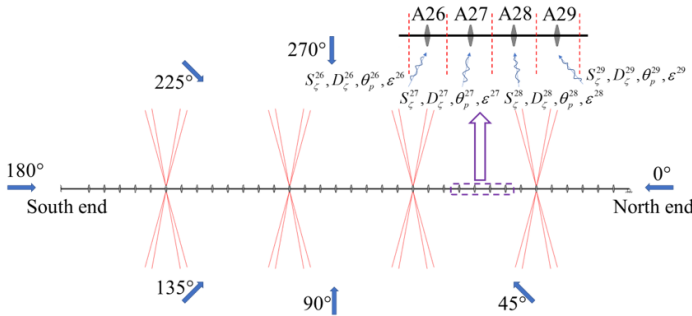

Fig.3: Description of inhomogeneous wave conditions along the floating bridge

Then, the spatial variation of wave characteristics (e.g. wave height H_s, peak period T_p and main wave direction θ_p) between the three DWRs is assumed to have a linear variation. As a basis for comparison, homogeneous wave conditions that are commonly used in practical engineering analysis and design are also considered. In view of the design wave load cases specified in the design basis (Statens vegvesen, 2018) and inhomogeneous wave data (Cheng et al., 2019a), 1-year design homogeneous and inhomogeneous wave conditions are listed in Tables 2 and 3, respectively. Note that the highest inhomogeneous H_s (at A27) is purposely made identical to the design homogeneous wave condition.

This is in line with the common practice in an engineering design in which the worst wave condition is often applied to the entire bridge structure.

It should be mentioned that the 1-year wave conditions are considered in this study due to the lack of detailed information regarding the wave inhomogeneity at the Bjørnafjord. They are employed as representative sea states for both structural response and fatigue analyses. Although harsher wave conditions, for example 100-year waves, are often used for ultimate limit state design checks, the analysis of the long-term joint distribution of the environmental conditions shows that the selected sea states are fairly extreme (Cheng et al., 2019b) and thus reasonable for evaluating the structural responses due to the wave inhomogeneity. The fatigue analysis presented in this paper is solely for the purpose of obtaining an indication of the inhomogeneous wave effect on the fatigue damage, in view of the fact that realistic fatigue damage evaluations depend on all possible wave conditions throughout the service life of the structure.

Table 4 lists the four load cases (LCs) to be examined in this study. Note that LC1 refers to the 1-year homogeneous wave load condition, while load cases 2-4 correspond to 1-year inhomogeneous wave load conditions. Besides the spatial variations of H_s and θ_p, the correlation of sea states at different pontoon locations, governed by the random phase angles of wave components ε^j (see Fig. 3), is also taken into account for inhomogeneous wave load cases. In this study, two conditions are analyzed. The first condition refers to fully coherent and correlated waves where the random phase angles of each wave component ε^j are identical at all pontoon locations. Essentially, this describes a fully continuous wave field. The second condition refers to uncorrelated waves at different pontoons locations by assigning different random phase angles for various pontoon locations ($\varepsilon^i \ne \varepsilon^j$ for arbitrary pontoon numbers i and j). Under such circumstances, the waves along the bridge length are completely independent and random.

Table 2. 1-year design homogeneous wave condition (Statens vegvesen, 2018)

H_s	T_p	θ_p
1.30 m	4.6 s	288°

Table 3. 1-year inhomogeneous wave condition

Loc.	H_s	T_p	θ_p	Loc.	H_s	T_p	θ_p
A1	1.17 m	4.6 s	314°	A19	1.24 m	4.6 s	298°
A2	1.17 m	4.6 s	314°	A20	1.25 m	4.6 s	297°
A3	1.17 m	4.6 s	313°	A21	1.25 m	4.6 s	295°
A4	1.17 m	4.6 s	312°	A22	1.26 m	4.6 s	294°
A5	1.17 m	4.6 s	311°	A23	1.27 m	4.6 s	293°
A6	1.18 m	4.6 s	310°	A24	1.28 m	4.6 s	292°
A7	1.18 m	4.6 s	310°	A25	1.29 m	4.6 s	290°
A8	1.18 m	4.6 s	309°	A26	1.29 m	4.6 s	289°
A9	1.18 m	4.6 s	308°	A27	1.30 m	4.6 s	288°
A10	1.19 m	4.6 s	307°	A28	1.29 m	4.6 s	286°
A11	1.19 m	4.6 s	307°	A29	1.29 m	4.6 s	284°
A12	1.19 m	4.6 s	306°	A30	1.28 m	4.6 s	281°
A13	1.19 m	4.6 s	305°	A31	1.27 m	4.6 s	279°
A14	1.20 m	4.6 s	304°	A32	1.26 m	4.6 s	277°
A15	1.21 m	4.6 s	303°	A33	1.25 m	4.6 s	275°
A16	1.22 m	4.6 s	301°	A34	1.25 m	4.6 s	272°
A17	1.22 m	4.6 s	300°	A35	1.24 m	4.6 s	270°
A18	1.23 m	4.6 s	299°				

Table 4. Description of load cases

Load case	Wave characteristics (H_s, T_p and θ_p)	Correlation
LC1	Homogeneous (Table 2)	Correlated
LC2	Homogeneous (Table 2)	Uncorrelated
LC3	Inhomogeneous (Table 3)	Correlated
LC4	Inhomogeneous (Table 3)	Uncorrelated

RESPONSE OF BRIDGE GIRDER

The bridge girder and the mooring lines are two key structural components of the floating bridge model. This section presents and discusses the dynamic responses of the bridge girder under the effect of homogeneous and inhomogeneous wave loads. The structural responses of the mooring lines and the corresponding fatigue damage estimation will be discussed in the following sections.

Figure 4 shows the statistical results, including the maximum responses and standard deviations, of the weak axis bending moment of the bridge girder M_y under homogeneous and inhomogeneous irregular wave conditions. Note that the maximum responses include the components due to the self-weight of the bridge structure. Results show that the effect of inhomogeneous wave loads significantly affects the standard deviations, which correspond to the dynamic components of M_y. This applies in particular to the segment between the south end and A27. Within this segment, inhomogeneous waves are more oblique than the homogeneous waves which are close to a beam sea condition. Consequently, wave excitation forces acting on the pontoons are larger for inhomogeneous wave load cases because of the pontoon geometry. Still, the extreme responses are found to be virtually unaffected by wave inhomogeneities, since they are mainly governed by the self-weight of the bridge girder.

The effect of inhomogeneous wave loads on the strong axis bending moment of the bridge girder, i.e. M_z, is shown in Fig. 5. In contrast to the M_y responses, the strong axis bending moment is insensitive to the wave inhomogeneities. Based on closer inspection of the bridge's modal properties, it is observed that unlike the vertical bending modes whose natural periods are mainly clusters around the wave periods, the fundamental transverse bending modes are sufficiently far away from the wave periods. Therefore, no significant resonance in M_y due to the excitation of wind waves is expected. Furthermore, it is expected that the wave short-crestedness has an effect in reducing the differences between homogeneous and inhomogeneous wave load cases when the wave inhomogeneity is mainly due to the spatial variation of wave directions. Consequently, the effect of inhomogeneous wave loads on M_z is found to be negligible.
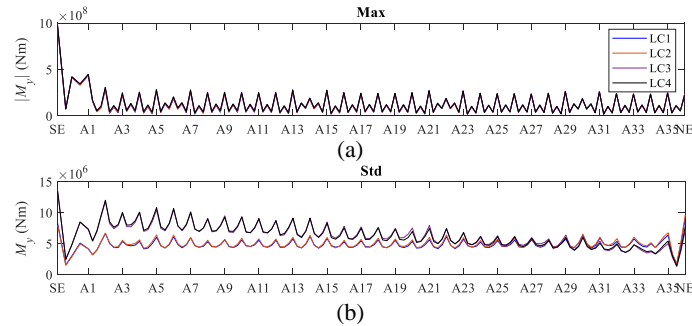

Fig.4: Weak axis bending moment of girder: (a) maximum responses and (b) standard deviations
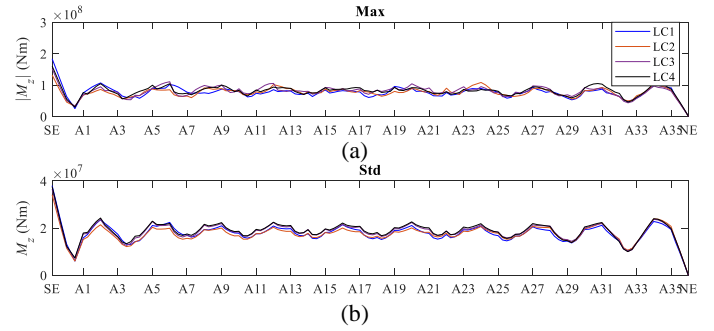

Fig.5: Strong axis bending moment of girder: (a) maximum responses and (b) standard deviations

The effect of inhomogeneous wave loads on the axial force F_x of the bridge girder is shown in Fig. 6. As can be seen, the inhomogeneous wave load cases induce much higher axial forces than LC1 for the segment between the south end and A27. Similar to M_y responses, the amplified axial responses are due to the fact that inhomogeneous waves are more oblique within this segment, leading to larger excitation forces exerted on the pontoons. After A27, the differences between all load cases are found to be small and F_x is observed to reduce rapidly to zero when approaching the north end due to the boundary condition.
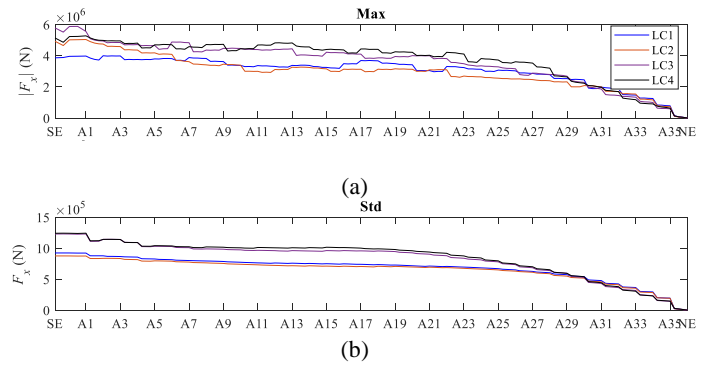

Fig.6: Axial force of girder: (a) maximum responses and (b) standard deviations

Figure 7 shows the torsional responses T of the bridge girder. Like M_z responses, inhomogeneous waves do not have a significant effect on the extreme values and standard deviations of T, although the induced responses are relatively higher than the homogeneous wave load case LC1. It is worth noting that the correlation between sea states affects the torsional responses considerably when there are no spatial variations of wave characteristics (H_s, T_p and θ_p). The uncorrelated case LC2 leads to larger torsional responses than the fully correlated case LC1. This indicates that the wave loads acting on pontoons with different phase angles for an uncorrelated case tends to result in larger torsional moments of the bridge girder, which is as expected. However, the effect of wave correlation is found to be smaller between LC3 and LC4. This may be explained as being due to the spatial variation of the direction angle θ_p, which also has an effect in amplifying the torsional responses similar to uncorrelated waves.
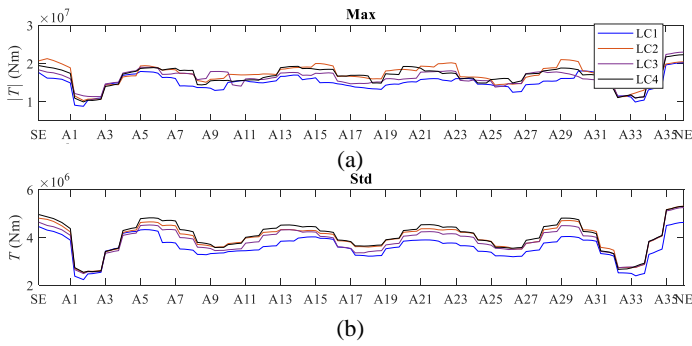
Fig.7: Torsional moment of girder: (a) maximum responses and (b) standard deviations

RESPONSE OF MOORING LINES

Besides the girder, mooring lines are also key structural components of the floating bridge. They effectively restrain the transverse motion of the bridge and add hydrodynamic viscous damping to the entire structure. Therefore, their dynamic responses are of great importance and worthy of investigation.

Figure 8 illustrates the four clusters of mooring lines and the numbering of each line. As the fairlead points are expected to sustain larger loads than the other parts of the mooring lines, this study focuses only on the responses at the fairlead.
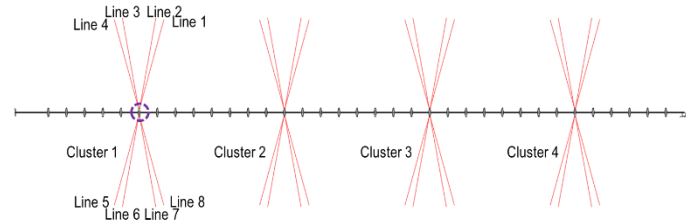
Fig. 8: Mooring system of floating bridge

Figure 9 plots the maximum mooring line tension at the fairlead. As can be seen, the extreme values are insensitive to inhomogeneous wave loads. This is due to the large initial pretension applied to the mooring lines. Nevertheless, the inhomogeneous load cases LC3 and LC4 generally tend to induce slightly larger tension than the homogeneous wave load case LC1, especially for mooring clusters 1 to 3. At the location of mooring cluster 4, both homogeneous and inhomogeneous wave load cases have very similar wave conditions. Consequently, the maximum mooring line tensions are virtually the same for all four load cases.
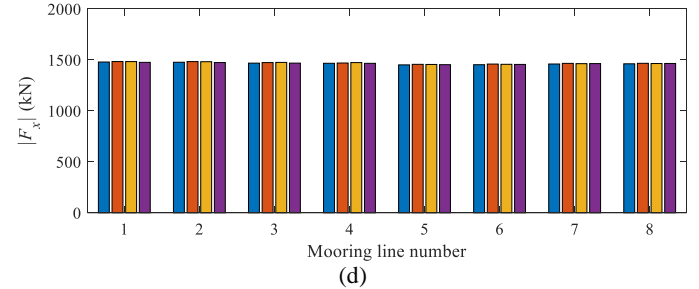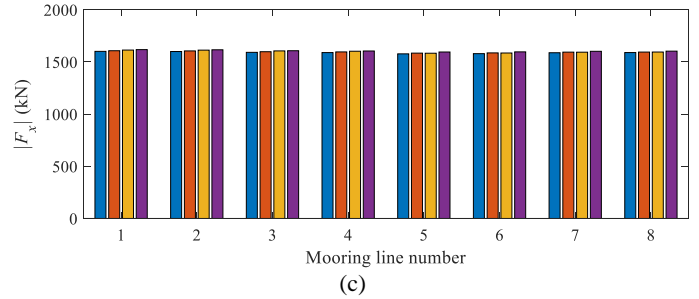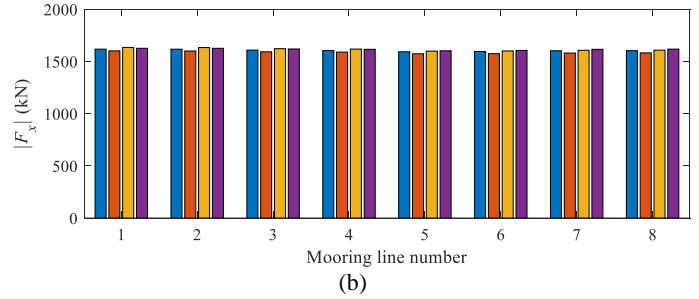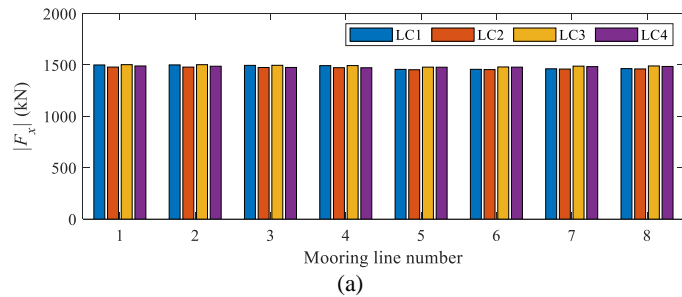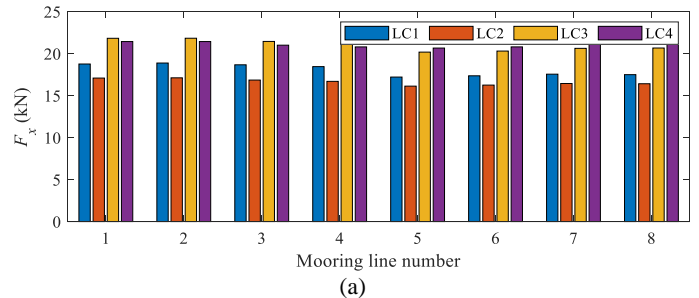

Fig. 9: Maximum mooring line tension at fairlead: (a) cluster 1, (b) cluster 2, (c) cluster 3 and (d) cluster 4

The standard deviations of mooring line tension, which characterize the dynamic components, are plotted in Fig. 10. In contrast to the extreme responses, the standard deviations are found to be substantially amplified by the inhomogeneities in the wave field, especially for mooring clusters 1 and 2. This is expected in view of the fact that inhomogeneous waves are more oblique (and thus higher excitation forces acting on pontoons) than homogeneous waves near these two mooring clusters. The obliquity of inhomogeneous waves reduces as it approaches mooring cluster 4 where a near beam sea condition forms. Consequently, homogeneous wave loads are found to induce larger standard deviations of mooring line tension than inhomogeneous wave loads, particularly for the mooring lines at the weather side.
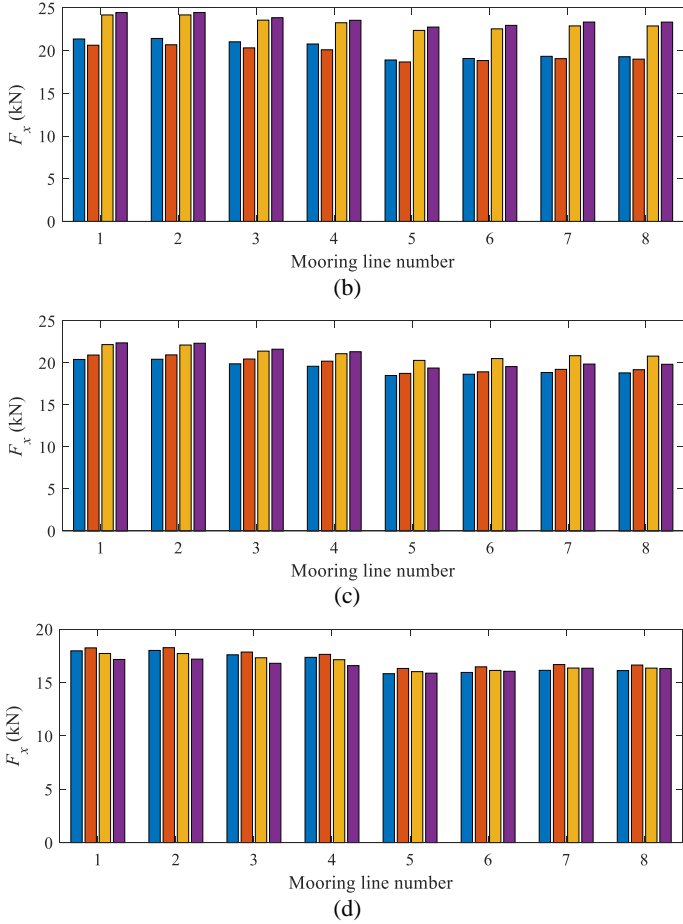
Fig. 10: Standard deviation of mooring line tension at fairlead: (a) cluster 1, (b) cluster 2, (c) cluster 3 and (d) cluster 4

FATIGUE DAMAGE IN MOORING LINES

The structural analysis results show that although the maximum mooring line tension is very similar for all four wave load cases considered in this study, inhomogeneous waves do induce higher standard deviations of tensile forces of most mooring lines. This indicates that the fatigue damage induced in the mooring lines may be larger when the waves are inhomogeneous. Thus, the fatigue damage caused by inhomogeneous wave loads is worthy of investigation.

It should be highlighted that a typical fatigue damage calculation includes all possible load cases throughout the service life of the structure under consideration. However, this is not possible for the current study as there is information on the spatial variations of waves characterizing only one inhomogeneous sea state due to the availability of data. Nevertheless, the response time series for a single sea state may still be used for the purpose of estimating the effect of inhomogeneous waves on fatigue damage and comparing it with results for the corresponding homogeneous wave load case. The purpose of this study is thus to obtain an indication of the effect of wave inhomogeneity on fatigue damage based on a limited number of sea states.

In the fatigue damage calculation, the computed mooring tension F_x is first converted to a nominal stress σ_n as

$$\sigma_n = \frac{F_x}{A_n} \tag{7}$$

where A_n is the nominal cross-sectional area of the mooring line. Note that the nominal diameter of the chain, which is 147 mm as listed in Table 1, also comprises a 20 mm corrosion allowance. For stress calculations, a 50% reduction in the corrosion allowance is accounted for. Also note that the effect of mean stress is neglected for the sake of simplicity. Then, the fatigue damage D is computed according to the Palmgren-Miner sum by using the rainflow counting algorithm as

$$D = \sum_{i=1}^{n} \frac{n_i}{K} S_i^m \tag{8}$$

where n_i is the number of cycles counted for stress range S_i, K and m are material parameters that characterize the relevant S-N curve of the material. For studless chains considered in this study, K and m are set to 6×10^{10} and 3, respectively (DNV GL, 2018).

Figure 11 shows the fatigue damage to mooring lines at the fairlead under homogeneous and inhomogeneous wave load cases. For each load case, the fatigue calculation is based on a three-hour simulation. As can be seen, the mooring lines in cluster 2 facing the weather side are subjected to larger fatigue damages than the other mooring clusters. It is also found that inhomogeneous wave loads significantly amplify the fatigue damage in mooring clusters 1 and 2. For example, the spatial variations of wave H_s and θ_p in LC3 caused fatigue damage to mooring line 8 in both clusters to be 70% higher than for the homogeneous wave load case LC1. When the waves are uncorrelated as for LC4, the difference further increases to about 80%. In the case of cluster 3 where the obliquity of the inhomogeneous waves decreases, the amplification due to inhomogeneous wave load cases reduces to 20-30%. This further decreases at cluster 4 where homogeneous wave load case LC1 is found to cause larger fatigue damages, especially for the mooring lines at the weather side.
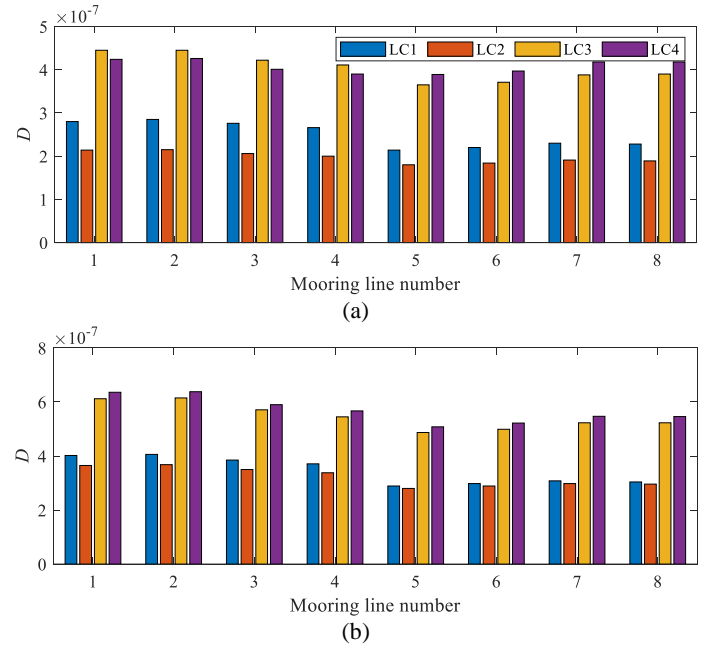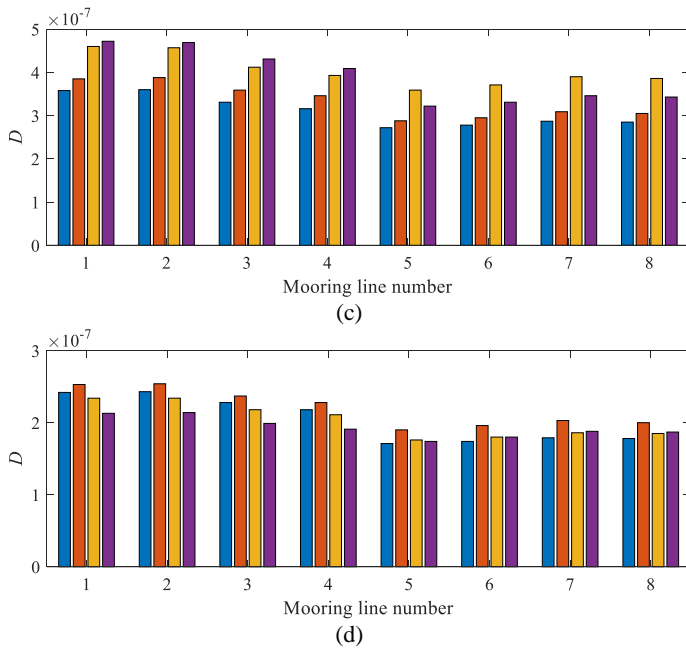
Fig. 11: Fatigue damage of mooring line at fairlead: (a) cluster 1, (b) cluster 2, (c) cluster 3 and (d) cluster 4

CONCLUSIONS

This paper presents a computation study of a very long, straight and side-anchored floating bridge for the crossing of the Bjørnfjord. The bridge girder is resting on 35 evenly spaced pontoons and is laterally restrained by four clusters of deep water mooring lines. According to available field measurement, the wave field along the floating bridge exhibits inhomogeneity. The effect of wave inhomogeneity on the structural responses of the bridge girder and mooring lines is examined. In addition, an indication of the effect of wave inhomogenity on the fatigue damage in the mooring lines is also obtained by considering a few sea states. Comparison with results for a homogeneous wave load case shows that employing homogeneous wave conditions in the analysis and design for the purpose of simplification could lead to underestimation of structural responses. This applies particularly to the weak axis bending moment of the bridge girder where the spatial variation of the wave heading plays a significant role. When it comes to the structural responses of mooring lines, the maximum responses are found to be insensitive to the wave inhomogeneity. However, the dynamic responses of the mooring tensions are substantially affected by the inhomogeneous wave loads. A study on the fatigue damage in mooring lines reveals that the inhomogeneous waves could lead to an amplification of the fatigue damage as large as 80%. Therefore, it is important that the wave inhomogeneity is properly measured/predicted and considered in the analysis to ensure that a safe design of the floating bridge.

REFERENCES

Cheng, Z, Gao, Z, and Moan, T (2018a). "Hydrodynamic load modeling and analysis of a floating bridge in homogeneous wave conditions," *Mar Struct*, 59, 122-141.

Cheng, Z, Gao, Z, and Moan, T (2018b). "Wave load effect analysis of a floating bridge in a fjord considering inhomogeneous wave conditions," *Eng Struct*, 163, 197-214.

Cheng, Z, Svangstu, E, Gao, Z, and Moan, T (2019a). "Field measurements of inhomogeneous wave conditions in Bjørnafjorden" *J Waterw Port Coast*, 145(1), 05018008.

Cheng, Z, Svangstu, E, Moan, T, and Gao, Z (2019b). "Long-term joint distribution of environmental conditions in a Norwegian fjord for design of floating bridges" *Ocean Eng*, 191, 106472.

COWI (2019). "Floating bridge over Bjørnafjord," https://www.cowi.com/solutions/infrastructure/bjoernafjord-ground-breaking-floating-bridge-for-a-ferry-free-e39-norway (accessed 30 Dec 2019).

Cummins, WE (1962). "The impulse response function and ship motions," Report No. DTMB-1661, Washington DC.

Dai, J, Leira, BJ, Moan, T, and Kvittem, MI (2020). "Inhomogeneous wave load effects on a long, straight and side-anchored floating pontoon bridge," *Mar Struct*, 72, 102763.

DNV GL (2018). "Bjørnafjorden side anchored floating bridge - independent global analyses," DNV GL, Oslo.

Fylling, IJ (2012). "Dynamisk analyse av flytebrukonsept for Sulesund – Hareid," MARINTEK Report No. 580319.

Gudmestad, OT, Moe, G (1996). "Hydrodynamic coefficients for calculation of hydrodynamic loads on offshore truss structures," *Mar Struct*, 9(8), 745-758.

Multiconsult (2017a). "Analysis and design (Base Case)," Multiconsult AS, Oslo.

Multiconsult (2017b). "Analysis and design (Base Case) Appendix I: Design of mooring lines," Multiconsult AS, Oslo.

Naess, A, Moan, T (2012). "Stochastic dynamics of marine structures," Cambridge University Press, New York.

SINTEF Ocean (2019a). "RIFLEX 4.16.0 Theory Manual," SINTEF Ocean, Trondheim.

SINTEF Ocean (2019b). "SIMO 4.16.0 Theory Manual," SINTEF Ocean, Trondheim.

Statens vegvesen (2018). "Design basis Bjørnafjorden rev E," Statens vegvesen, Oslo.

Viuff, T, Leira, BJ, Xiang, X, and Øiseth O (2019). "Effects of wave directionality on extreme response for a long end-anchored floating bridge," *Appl Ocean Res*, 90, 101843.

WAMIT (2019). "WAMIT User Manual Version 7.3," WAMIT, Chestnut Hill.

Xiang, X, Viuff, T, Leira, BJ, Øiseth O (2018). "Impact of hydrodynamic interaction between pontoons on global responses of a long floating bridge under wind waves," *Proc 37th Int Conf Ocean, Offshore and Arctic Eng*, Madrid, ASME.